



Article

# Aluminum-Alumina Composites: Part I: Obtaining and Characterization of Powders

Alexander A. Gromov <sup>1</sup>, Anton Yu. Nalivaiko <sup>1,\*</sup> , Grayr N. Ambaryan <sup>2</sup>, Mikhail S. Vlaskin <sup>2</sup> , Olesya A. Buryakovskaya <sup>2</sup>, Sergey A. Kislenco <sup>2</sup>, Andrey Z. Zhuk <sup>2</sup>, Evgeniy I. Shkolnikov <sup>2</sup>, Konstantin V. Slyusarskiy <sup>1</sup>, Alexandra A. Osipenkova <sup>1</sup> and Alexey N. Arnautov <sup>1</sup>

<sup>1</sup> KINETICA Engineering Center, National University of Science and Technology MISIS, 119991 Moscow, Russia; a.gromov@misis.ru (A.A.G.); slyuskonst@gmail.com (K.V.S.); 79859100168@ya.ru (A.A.O.); aleksej.arnautov@gmail.com (A.N.A.)

<sup>2</sup> Laboratory of Energy Storage Substances, Joint Institute for High Temperatures of the Russian Academy of Sciences, 125412 Moscow, Russia; ambaryan1991@gmail.com (G.N.A.); vlaskin@inbox.ru (M.S.V.); osminojishe@ya.ru (O.A.B.); kislenco-s@mail.ru (S.A.K.); 666zhuk@ihed.ras.ru (A.Z.Z.); 2shkolnikov@ihed.ras.ru (E.I.S.)

\* Correspondence: nalivaiko@misis.ru; Tel.: +7-499-700-0306 (ext. 50703)

Received: 29 August 2019; Accepted: 26 September 2019; Published: 27 September 2019



**Abstract:** The process of advanced aluminum-alumina powders production for selective laser melting was studied. The economically effective method of obtaining aluminum-alumina powdery composites for further selective laser melting was comprehensively studied. The aluminum powders with 10–20 wt. % alumina content were obtained by oxidation of aluminum in water. Aluminum oxidation was carried out at  $\leq 200$  °C. The oxidized powders were further dried at 120 °C and calcined at 600 °C. Four oxidation modes with different process temperatures (120–200 °C) and pressures (0.15–1.80 MPa) were investigated. Parameters of aluminum powders oxidation to obtain composites with 10.0, 14.5, 17.4, and 20.0 wt. % alumina have been determined. The alumina content, particle morphology, and particle size distribution for the obtained aluminum-alumina powdery composites were studied by XRD, SEM, laser diffraction, and volumetric methods. According to the obtained characteristics of aluminum-alumina powdery composites, they are suitable for the SLM process.

**Keywords:** aluminum; alumina; composite; powder; oxidation; selective laser melting; particle morphology

## 1. Introduction

Selective laser melting (SLM) for 3D metal object production is a rapidly developing field of science and technology. 3D printing of aluminum alloys and aluminum matrix composites (AMC) is pretending to become the leading technology for the production of complex shape details for aerospace and automotive engineering [1–7].

The SLM process parameters (laser power, scanning speed, powder feeding rate, etc.) have a decisive influence on the 3D object characteristics [8–11]. The quality of the initial powder is quite significant as well [12,13]. The properties of aluminum-based alloys are well suited to produce complex shape objects of high strength and density by SLM processes [14].

There are many problems in structure formation (for example, porosity) of 3D sintered objects formed by using the powders with a broad particle size distribution. The powders with spherical particles having a narrow size distribution is the best initial material to obtain 3D objects with high quality by SLM. This provides a compact packaging of particles in a melted layer and a stable feeding rate of the powder. For example, aluminum powders with a particle size from 30 to 100  $\mu\text{m}$  are typically used for 3D printing by the SLM process [15,16].

Disadvantages of aluminum powders for additive technologies are their poor flowability, low emissivity factor, high conductivity, and low mechanical properties of synthesized 3D objects [17,18]. On the opposite side, aluminum powders reinforced with refractory additives allow to obtain sintered objects with excellent properties, such as good wear resistance, high hardness, and tensile strength [19]. In such powders, aluminum is the matrix phase and it forms a percolating network during sintering, and the refractory additive is the reinforcement and crystallization center [20]. SiC, TiC, TiB<sub>2</sub>, or Al<sub>2</sub>O<sub>3</sub> can be used as a refractory additive [21]. However, the use of Al<sub>2</sub>O<sub>3</sub> eliminates the possibility of formation of side phases during sintering and interaction of the reinforcement with the aluminum matrix. aluminum-alumina composites are considered as raw materials for the synthesis of potential lightweight and high-strength alloys for aircraft and automotive industry [19].

Aluminum particles covered with an alumina shell (Al core and Al<sub>2</sub>O<sub>3</sub> shell) is an interesting raw material for 3D printing. The Al core and Al<sub>2</sub>O<sub>3</sub> shell structure of the particles has higher stability, emissivity, thermal resistance, and aging properties in comparison with non-oxidized aluminum particle [22]. The flowability of such powder is also much higher due to lower surface energy and, as a result, lesser cohesion forces. Despite some advantages, high aluminum oxide content in the obtained object could decrease its strength properties. That is why alumina content in composites should be strictly controlled.

There are different ways of obtaining aluminum-alumina powder composites from aluminum powder. The most obvious is the oxidation of aluminum by air or oxygen [23–25]. However, the oxidation of small particles causes the formation of hollow alumina spheres [23]. As the initial material for the SLM process, hollow alumina has unacceptable characteristics (see Figure 1). Oxidation of aluminum powder in water is one of the possible solutions [26,27]. The aluminum particle oxidation process can be stopped at any oxidation degree by reagent separation (water and aluminum) at a certain time. The oxidized powder can be deleted from the water by filtering or sedimentation. This method is perfectly suitable for producing Al core and Al<sub>2</sub>O<sub>3</sub> shell powdery composites.

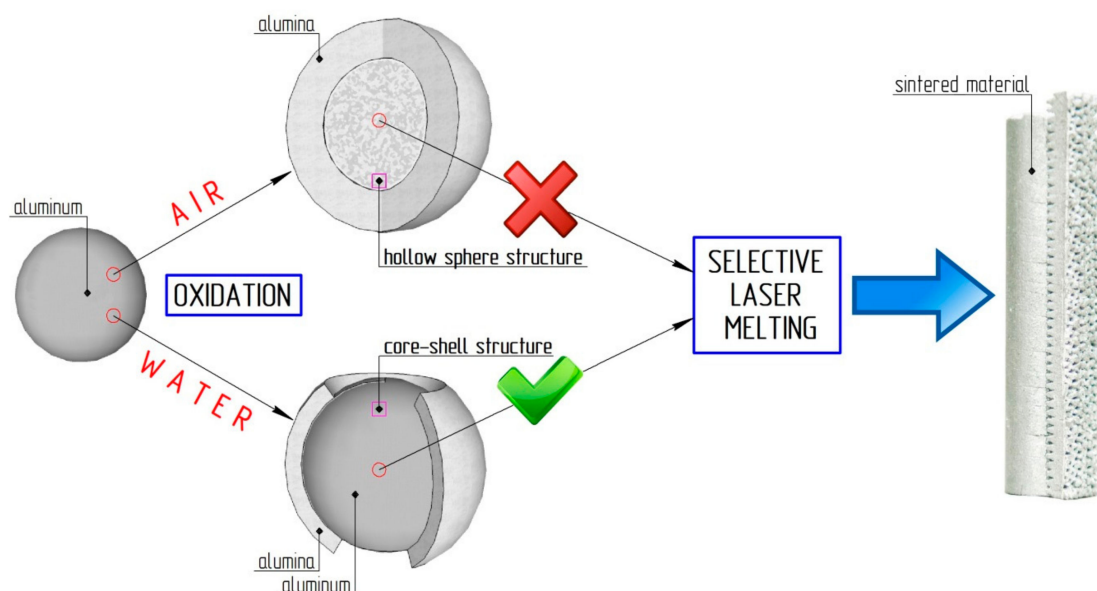


**Figure 1.** Scheme of the slow oxidation of aluminum particle by air and water.

The oxidation of nano- and micron-sized aluminum powders by water is widely studied [22,23,26–33]. The majority of publications [22,28–31,34] dealt with the different points of obtaining hydrogen by the reaction of aluminum with water. The primary purpose of such works is an increase in the Al + H<sub>2</sub>O reaction rate because aluminum is passivated by oxide layer [26,31,34]. Many works on the aluminum powder oxidation by water and steam are devoted to the theoretical aspects of the aluminum oxidation and hydrogen obtaining [28,34]. Some studies have shown that high oxidation temperatures lead to the

following problems: Poorly ordered crystal structure of oxidation products, agglomeration of particles, low specific surface area and micropores in oxidation products [31]. The effect of mechanochemical activation on the reaction kinetics in Al–H<sub>2</sub>O system was studied, and the effect of alkali metals was investigated [22,28–30]. The oxidation of the micron-sized aluminum powder by water for the synthesis of pore-free aluminum-alumina composites was also proposed [35]. This oxidation leads to the formation of aluminum particles with an oxide surface layer (Al core and Al<sub>2</sub>O<sub>3</sub> shell) [28,31,36].

The aim of this work is to study the process of oxidation of aluminum with water for the manufacture of Al core and Al<sub>2</sub>O<sub>3</sub> shell powder composites and the obtained powder's comprehensive characterization.

## 2. Materials and Methods

### 2.1. Aluminum Powder

Micron-sized aluminum powder (purchased from RUSAL Co., Russia) was used as the initial material to obtain aluminum-alumina composite. Aluminum powder was produced by molten aluminum spraying. The elemental composition of aluminum powder was studied by using the ThermoScientific X-2 mass spectrometer with inductively coupled plasma gun (ICP-MS method). The powder size distribution curves were obtained with the Fritsch Analysette 22 particle size analyzer.

### 2.2. Aluminum-Alumina Powder Composites

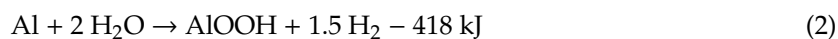
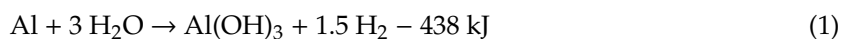
The method of obtaining the aluminum-alumina composite powder consisted of two stages:

1. Oxidation of aluminum powder by water at pressure 0.15–1.80 MPa;
2. Powder drying at 120 °C and calcination of the aluminum-alumina composite in a furnace at 600 °C.

#### 2.2.1. Oxidation of Aluminum Powder by Water (Stage 1)

The first stage of obtaining the aluminum-alumina powder composites was the oxidation of aluminum powder by water. The oxidation process was executed in the high-pressure reactor which was described in [37]. Three kilograms of suspension of aluminum powder and distilled water (mass ratio of H<sub>2</sub>O/Al = 2) was added into the reactor. The reactor had a volume of five liters, and it was made of stainless steel with Teflon thermal isolation inside. An anchor-type agitator with 100 rotations per minute stirred the suspension continuously.

The temperature and the pressure inside the reactor were controlled by thermocouple type K (Ni–CrNi) and pressure sensor. When the pressure and temperature values were above a certain limit, additional cool water was added to the reactor to reduce its temperature. High heating is associated with the exothermic reaction of aluminum oxidation, which emits from 418 to 438 kJ/(mol Al) of heat (Equations (1) and (2))



The H<sub>2</sub>O/Al suspension was poured into the reactor, and the suspension was continuously mixed. The suspension was heated at 3 K/min rate to a certain temperature (see Table 1). The mixture of hydrogen and steam was transferred to the heat exchanger where the water was condensed and returned to the reactor. Hydrogen was a byproduct, and it was released into the atmosphere. Solid products of the reaction (Al + Al(OH)<sub>3</sub> + AlOOH) were removed from the bottom of the reactor. The resulting solid reaction products (Al + Al(OH)<sub>3</sub> + AlOOH) were separated from the residual water by the filtration process.

**Table 1.** Parameters of obtaining aluminum-alumina powdery composites.

Mode	Parameters of Stage 1				
	Maximal Temperature, °C	Pressure, MPa	Volume of the Released H <sub>2</sub> , Liters	Alumina Content, wt. %	Mean Alumina Layer Thickness *, μm
A	120	0.15	65	10.0	1.45
B	180	1.35	190	14.5	2.14
C	190	1.50	260	17.4	2.60
D	200	1.80	300	20.0	3.00

\*: Calculated for mean particle diameter particle.

### 2.2.2. Drying and Calcination (Stage 2)

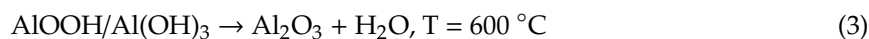
The thermal treatment consisted of drying and calcination.

The wet powder from Stage 1 (Al + Al(OH)<sub>3</sub> + AlOOH) was loaded into stainless steel containers. The container was placed in the Binder VD drying box. The drying process was executed for 1 h at 120 °C.

Then, the dried powder was subjected to the calcination. This stage was necessary for the conversion of all crystalline modifications of oxidation products (Al(OH)<sub>3</sub>, AlOOH, etc.) to γ-Al<sub>2</sub>O<sub>3</sub>. The calcination process was carried out for five hours at 600 °C (LHT 08/16 Nabertherm laboratory furnace).

### 2.2.3. Characterization

Products of chemical interaction of powdery aluminum with water (reactions (1) and (2)) were identified in [28]. Reactions (1) and (2) were proceeded in parallel depending on the process temperature. According to [22], oxidation products after Stage 1 were presented by Al(OH)<sub>3</sub>, AlOOH, and θ-Al<sub>2</sub>O<sub>3</sub>. The possibility of γ-Al<sub>2</sub>O<sub>3</sub> formation from reactions 1 and 2 was not reported. Further thermal treatment was needed to convert aluminum hydroxides into the aluminum oxides (3).



The alumina content in the resulting aluminum-alumina powdery composites was determined by the amount of hydrogen, which was released during the oxidation of aluminum powder by water. However, aluminum-alumina composites were further oxidized during the calcination process. Therefore, the aluminum content in the finally obtained composites was determined by the volumetric method [25].

The morphological properties of the finally obtained aluminum-alumina composites were studied on the JEOL JSM-7407F microscope. The phase composition of the composites was studied by the EQUINOX 1000 X-ray diffractometer.

## 3. Results

### 3.1. Aluminum Powder Characterization

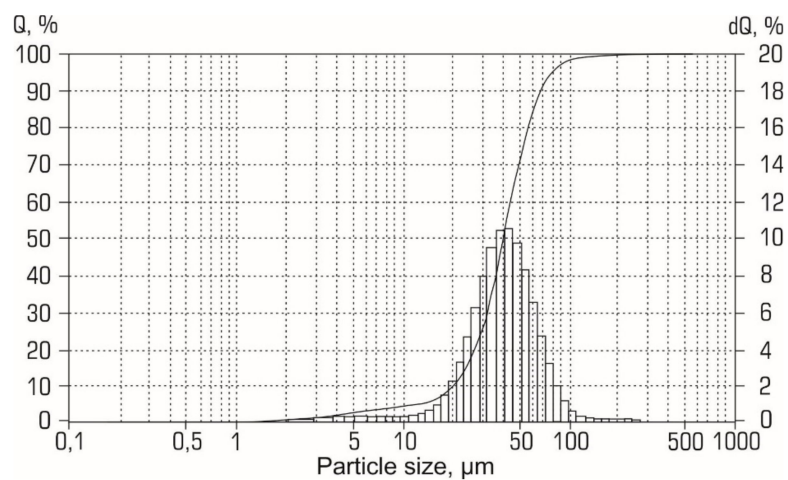
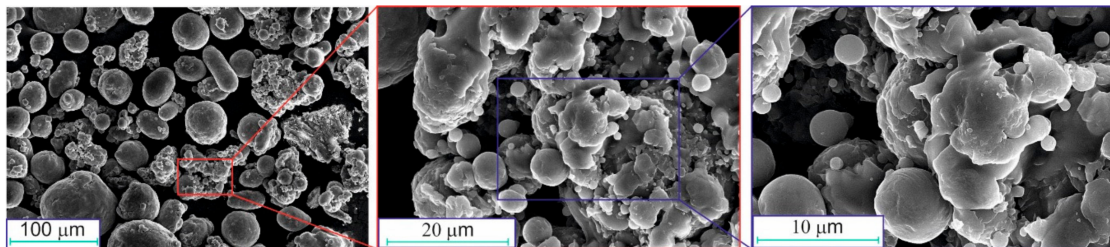
The elemental composition of the initial aluminum powder is presented in Table 2. The most significant impurities were Ga (0.09 wt. %), Zn and Ce (both 0.08 wt. %), Fe, and La (both 0.07 wt. %). According to the size distribution curves (see Figure 2), the particles of the initial Al powder had a diameter from 1 to 120 μm.

SEM images of the initial aluminum powder are shown in Figure 3. The particles were spherical or spheroidal. Several agglomerates consisting of smaller spherical particles were observed.

Thus, the low impurities content together with the relatively narrow particle size distribution and spherical particles' shape makes this initial aluminum powder suitable as a raw material for further oxidation and core-shell composites preparation.

**Table 2.** Parameters of obtaining aluminum-alumina powdery composites.

Element, wt. %	
Al	99.20
Ga	0.09
Zn	0.08
Ce	0.08
La	0.07
Fe	0.07
V	0.03
Mg	0.02
B	0.01
Cr, Ti, Co, Y, Cu, and volatiles	0.35

**Figure 2.** Size distribution curve for the initial aluminum powder.**Figure 3.** SEM images of the initial aluminum powder.

### 3.2. Oxidation of Aluminum Powder

Four oxidation modes were studied to obtain aluminum-alumina powdery composites with the alumina content from 10.0 wt. % for mode A (see Figure 4a) to 20.0 wt. % for mode D (see Figure 4d and Table 1). The higher amount of released hydrogen for mode D compared to mode A corresponded to a higher alumina content in the powder. The higher alumina content correlated with the higher oxidation temperature and longer reaction time (see Figure 4). According to Figure 4, oxidation of aluminum by water was initiated at a temperature of about 68 °C. This can be explained by the partial permeability of the surface oxide layer at this temperature.

The curves of hydrogen yield (Figure 4) had approximately the same slope for all studied oxidation modes. The oxidation rate was increased linearly as the oxidation temperature increased. The reason for that was the active self-sustaining exothermic reaction of aluminum with water, which has been reported in numerous publications [22,30,31,34]. For the studied modes, the suppression of the reaction rate due to the protective layer formation on aluminum particles was not found.

The alumina content in composites directly depended on the oxidation duration: For mode A the oxidation duration was 30 min and the alumina content was 10 wt.%. For mode D, the oxidation duration was 140 min and the alumina content was 20 wt.%.

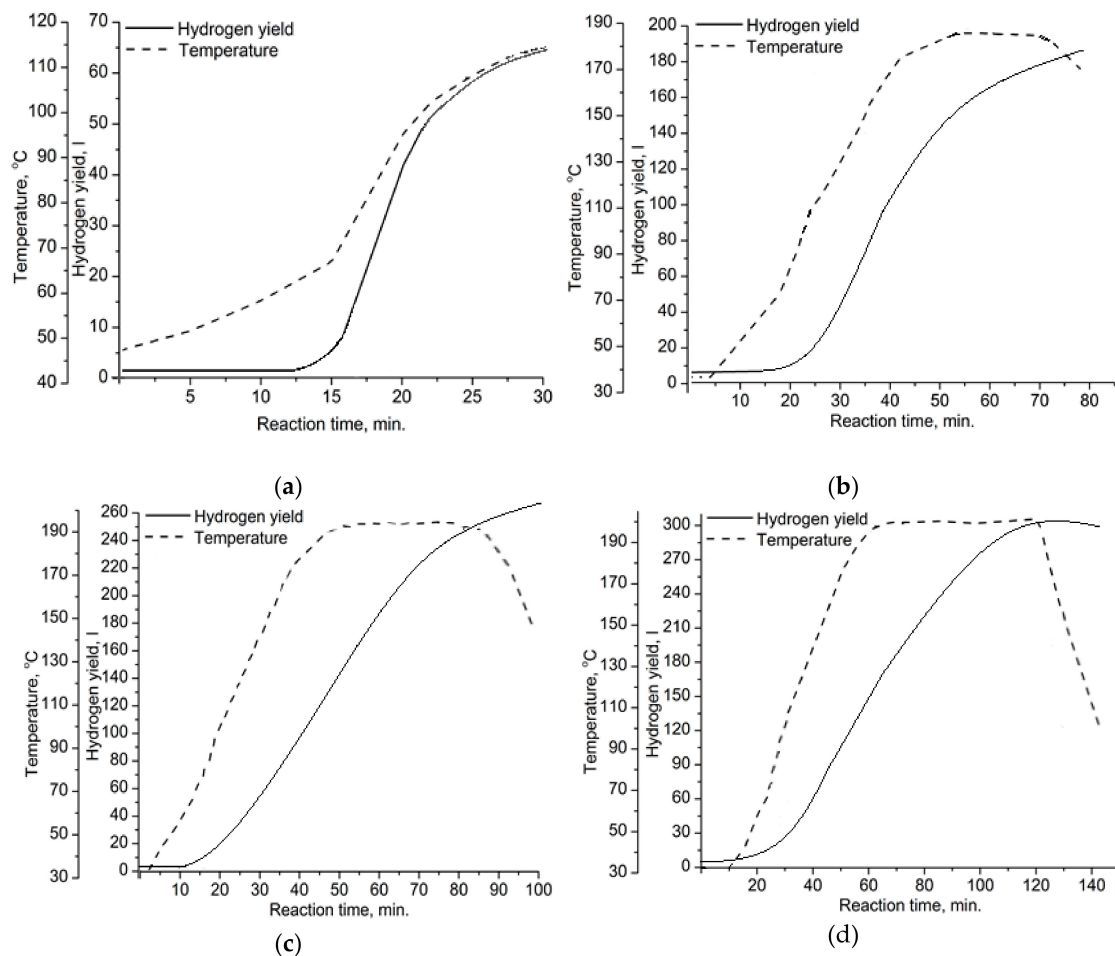


**Figure 4.** Yield of the released hydrogen and reaction temperature vs. reaction time for the following oxidation modes: (a) A, (b) B, (c) C, (d) D.

### 3.3. Effect of the Oxidation Mode on the Particles' Properties

SEM images of the obtained aluminum-alumina powdery composites (before drying and calcination) are shown in Figure 5.

Comparison of the images in Figures 3 and 5 shows that aluminum particles did not change their spherical shape after oxidation in water. The relatively smooth surface of aluminum particles was covered with a gibbsite-boehmite layer of oxidation products (see Figure 5a, right image). The hydroxide layer on the particles had an irregular structure formed by plate crystals (Figure 5a). Agglomerates of particles were also observed. The size of these agglomerates was larger than 100  $\mu\text{m}$  (see Figure 5b, left image) and they were larger than the average diameter of Al particles (see Figure 3, left image).

After deep oxidation (mode D), the aluminum particles did not change their shape (see Figure 5b). A small part of the hydroxide layer was separated from the surface, and individual particles were present in the sample (see Figure 5b, right image). The hydroxide layer on the particles oxidized in mode D consists of larger crystals, and it looks denser.

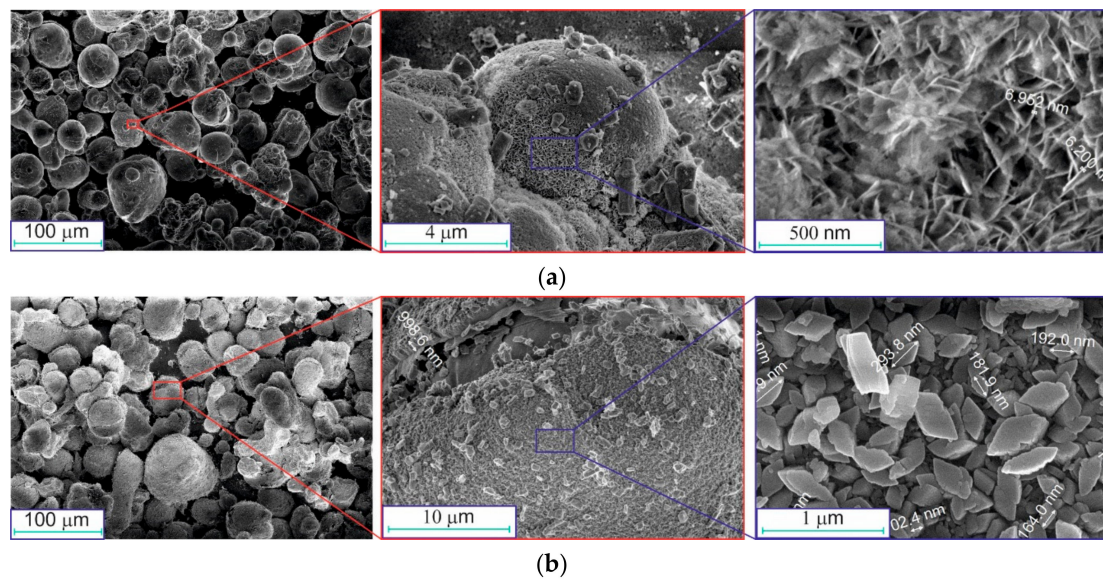


**Figure 5.** SEM images of the oxidized aluminum powders at different modes (before drying and calcination): (a) A, (b) D.

SEM images of aluminum-alumina powdery composites after heat treatment are shown in Figure 6. The particles were predominantly spherical. Nevertheless, there were some agglomerates, which are explained by the sintering of particles during the calcination process. After the deep oxidation (mode D) there were no agglomerates (see Figure 6b). A thicker oxide surface layer was preventing the sintering of particles. The presence of agglomerates had a little effect on the particle size distribution.

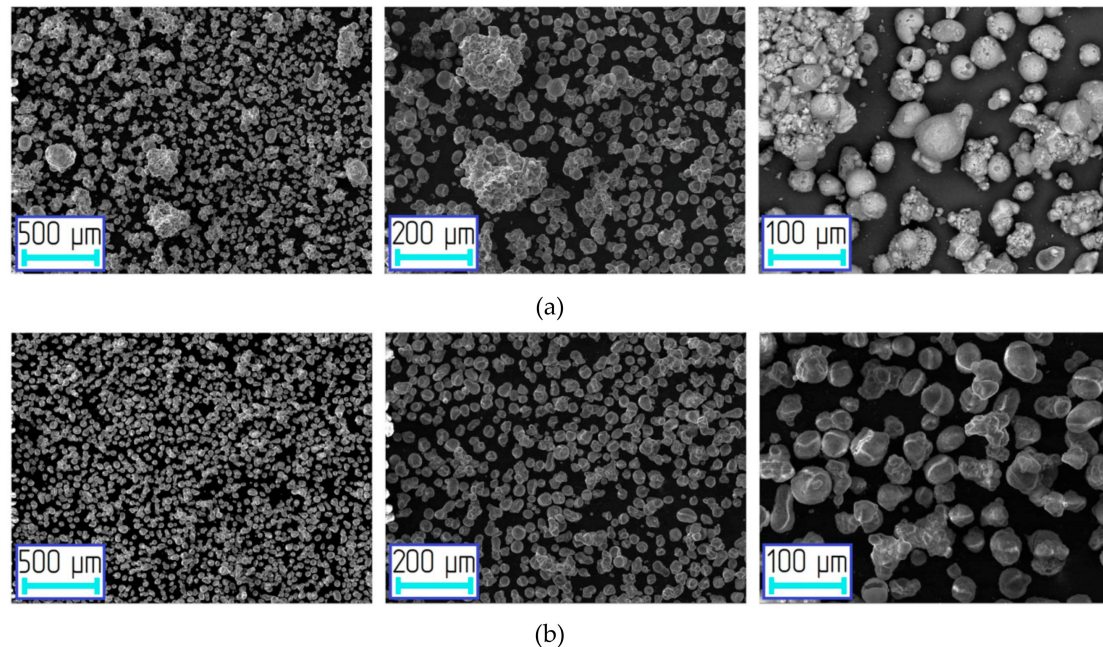


**Figure 6.** SEM images of the oxidized aluminum powders at different modes (after drying and calcination processes): (a) A, (b) D.

XRD patterns for the aluminum-alumina powdery composites (after heating and calcination) for the different alumina contents are shown in Figure 7. Analysis of XRD patterns shows that in addition to aluminum, the presence of  $\gamma\text{-Al}_2\text{O}_3$  was found. The relative intensity of the peaks corresponding to  $\gamma\text{-Al}_2\text{O}_3$  correlates with the alumina content of the aluminum-alumina powdery composites. Absence of any other crystalline phase in the aluminum-alumina powdery composites

was observed. Particle size distribution curves for aluminum-alumina powdery composites with alumina content of 10.0 wt. % and 20.0 wt. % are shown in Figure 8. Both powders (see Figure 8) have a rather narrow particle size distribution. More than 90% of the particles have a size from 20 to 80  $\mu\text{m}$ . In general, the size distribution curves of aluminum-alumina powdery composites were the same as for the initial aluminum powders (see Figure 2).

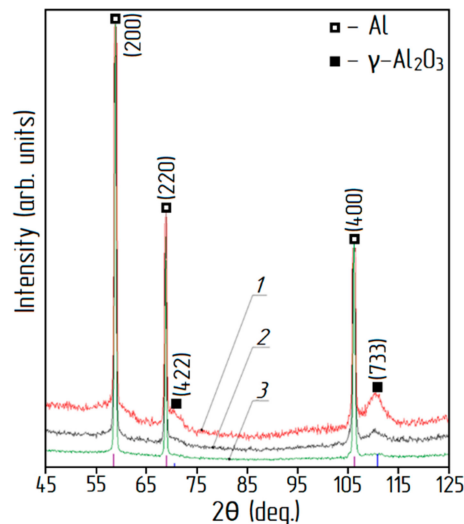


**Figure 7.** XRD patterns of aluminum-alumina powdery composites: 1) 20.0 wt. %  $\text{Al}_2\text{O}_3$ , 2) 14.5 wt. %  $\text{Al}_2\text{O}_3$ , 3) 10.0 wt. %  $\text{Al}_2\text{O}_3$ .

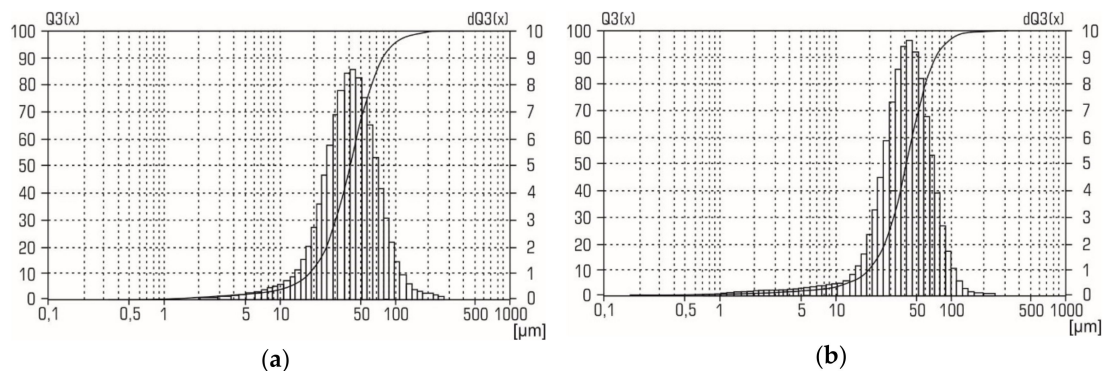


**Figure 8.** Particle size distribution of aluminum-alumina powder composites with the alumina content a) 10.0 wt. % and b) 20.0 wt. %.

The average particle size of aluminum-alumina composites was 41–42  $\mu\text{m}$ . This value was also average for the initial aluminum powder (see Figure 2). The calculated value mean oxide film thickness for average particle varied from 1.5  $\mu\text{m}$  (mode A) to 3  $\mu\text{m}$  (mode D) (Figure 5). A small change in the particle size distribution curves was, probably, due to the swelling of the particles because of the lower density of the oxide layer compared to aluminum. This could be explained by the absence of pores in the obtained powders. This is a significant advantage in comparison with partially oxidized powers in gaseous (oxygen, carbon dioxide) mediums which usually have a large pore volume [24,38].

#### 4. Conclusions

The method of obtaining aluminum-alumina powdery composites for their subsequent sintering by selective laser melting has been studied. Initial micron-sized aluminum powders were oxidized in water at 120–200  $^{\circ}\text{C}$  and 0.15–1.8 MPa pressure. Oxidation products were dried at 120  $^{\circ}\text{C}$  and calcined at 600  $^{\circ}\text{C}$ . Four high-pressure high-temperature oxidation modes were considered. The alumina content,



particle morphology, and particle size distribution for the obtained aluminum-alumina powdery compositions were studied by XRD, SEM, laser diffraction, and volumetric methods.

The temperature of the oxidation process affected the alumina content in the composites. The alumina content was 10.0 wt. % for 120 °C and it was increased to 20.0 wt. % at 200 °C. The beginning of the oxidation reaction of aluminum for all modes was observed at 68 °C.

The particles of the initial aluminum powder had a spherical shape and did not change significantly after processing. The average particle size and size distribution did not differ significantly from the initial aluminum powder indicating low porosity of the formed oxide layer. According to the obtained characteristics of aluminum-alumina powdery composites, they are suitable for further sintering. However, for the removal of agglomerates and additional sieving with 100 µm mesh size is necessary.

Synthesis of 3D objects from aluminum-alumina powdery composites by the SLM process will be considered in the future.

**Author Contributions:** Conceptualization, A.G. and A.N.; data curation, G.A. and O.B.; formal analysis, A.A.; investigation, M.V., A.Z. and E.S.; methodology, S.K.; resources, A.A.; supervision, A.G.; visualization, K.S. and A.O.; writing—original draft, K.S.; writing—review & editing, A.N.

**Funding:** The work is financially supported by Russian Science Foundation (RSF), grant № 19-79-30025.

**Acknowledgments:** The authors thank the MISIS Academic Writing University Center for its assistance in the preparation of this manuscript.

**Conflicts of Interest:** The authors declare no conflict of interest.

## References

1. Eyers, D.R.; Potter, A.T. Industrial Additive Manufacturing: A manufacturing systems perspective. *Comput. Ind.* **2017**, *92*, 208–218. [[CrossRef](#)]
2. Rauch, E.; Unterhofer, M.; Dallasega, P. Industry sector analysis for the application of additive manufacturing in smart and distributed manufacturing systems. *Manuf. Lett.* **2017**, *120*, 305–326. [[CrossRef](#)]
3. Kok, Y.; Tan, X.P.; Wang, P.; Nai, M.L.S.; Loh, N.H.; Liu, E.; Tor, S.B. Anisotropy and heterogeneity of microstructure and mechanical properties in metal additive manufacturing: A critical review. *Mater. Des.* **2018**, *139*, 565–586. [[CrossRef](#)]
4. Herzog, D.; Seyda, V.; Wycisk, E.; Emmelmann, C. Additive manufacturing of metals. *Acta Mater.* **2016**, *117*, 371–392. [[CrossRef](#)]
5. Szemkus, S.; Kempf, B.; Jahn, S.; Wiehl, G.; Heringhaus, F.; Rettenmayr, M. Laser additive manufacturing of contact materials. *J. Mater. Process. Technol.* **2018**, *252*, 612–617. [[CrossRef](#)]
6. Riberio, F. 3D printing with metals. *Comput. Control Eng. J.* **1998**, *9*, 31–38. [[CrossRef](#)]
7. Xu, W.; Brandt, M.; Sun, S.; Elambasseril, J.; Liu, Q.; Latham, K.; Xia, K.; Qian, M. Additive manufacturing of strong and ductile Ti-6Al-4V by selective laser melting via in situ martensite decomposition. *Acta Mater.* **2015**, *85*, 74–84. [[CrossRef](#)]
8. Martin, J.H.; Yahata, B.D.; Hundley, J.M.; Mayer, J.A.; Schaedler, T.A.; Pollock, T.M. 3D printing of high-strength aluminum alloys. *Nature* **2017**, *549*, 365–369. [[CrossRef](#)] [[PubMed](#)]
9. Kaufmann, N.; Imran, M.; Wischeropp, T.M.; Emmelmann, C.; Siddique, S.; Walther, F. Influence of Process Parameters on the Quality of Aluminum Alloy EN AW 7075 Using Selective Laser Melting (SLM). *Phys. Procedia* **2016**, *83*, 918–926. [[CrossRef](#)]
10. Ding, Y.; Muñoz-Lerma, J.A.; Trask, M.; Chou, S.; Walker, A.; Brochu, M. Microstructure and mechanical property considerations in additive manufacturing of aluminum alloys. *MRS Bull.* **2016**, *41*, 745–751. [[CrossRef](#)]
11. Gu, H.; Gong, H.; Dilip, J.J.S.; Pal, D.; Hicks, A.; Doak, H.; Stucker, B. Effects of Powder Variation on the Microstructure and Tensile Strength of Ti-6Al-4V Parts Fabricated by Selective Laser Melting. *Int. J. Powder Metall.* **2015**, *51*, 470–483.
12. Yin, S.; Yan, X.; Chen, C.; Jenkins, R.; Liu, M.; Lupoi, R. Hybrid additive manufacturing of Al-Ti6Al4V functionally graded materials with selective laser melting and cold spraying. *Mater. Process. Technol.* **2018**, *255*, 650–655. [[CrossRef](#)]

13. Liu, B.; Wildman, R.; Tuck, C.; Ashcroft, I.; Hague, R. Investigating the effect of particle size distribution on processing parameters optimisation in selective laser melting process. In Proceedings of the 22nd Annual International Solid Freeform Fabrication Symposium—An Additive Manufacturing Conference, Austin, TX, USA, 8–10 August 2011; pp. 227–238.
14. Zhang, H.; Zhu, H.; Qi, T.; Hu, Z.; Zeng, X. Selective laser melting of high strength Al–Cu–Mg alloys: Processing, microstructure and mechanical properties. *Mater. Sci. Eng. A* **2016**, *656*, 47–54. [[CrossRef](#)]
15. Pozdniakov, A.V.; Churyumov, A.Y.; Loginova, I.S.; Daubarayte, D.K.; Ryabov, D.K.; Korolev, V.A. Microstructure and properties of novel AlSi11CuMn alloy manufactured by selective laser melting. *Mater. Lett.* **2018**, *225*, 33–36. [[CrossRef](#)]
16. Manca, D.R.; Churyumov, A.Y.; Pozdniakov, A.V.; Ryabov, D.K.; Korolev, V.A.; Daubarayte, D.K. Novel heat-resistant Al–Si–Ni–Fe alloy manufactured by selective laser melting. *Mater. Lett.* **2019**, *236*, 676–679. [[CrossRef](#)]
17. Sercombe, T.B.; Li, X. Selective laser melting of aluminium and aluminium metal matrix composites: Review. *Mater. Technol.* **2016**, *31*, 77–85. [[CrossRef](#)]
18. Yu, W.H.; Sling, S.L.; Chua, C.K.; Kuo, C.N.; Tian, X.L. Particle-reinforced metal matrix nanocomposites fabricated by selective laser melting: A state of the art review. *Prog. Mater. Sci.* **2019**, *104*, 330–379. [[CrossRef](#)]
19. Durai, T.G.; Das, K.; Das, S. Synthesis and characterization of Al matrix composites reinforced by in situ alumina particulates. *Mater. Sci. Eng. A* **2007**, *445–446*, 100–105. [[CrossRef](#)]
20. Surappa, M.K. Aluminium matrix composites: Challenges and opportunities. *Sadhana* **2003**, *28*, 319–334. [[CrossRef](#)]
21. Pramod, S.L.; Bakshi, S.R.; Murty, B.S. Aluminum-Based Cast In Situ Composites: A Review. *J. Mater. Eng. Perform.* **2015**, *24*, 2185–2207. [[CrossRef](#)]
22. Tikhov, S.F.; Fenelonov, V.B.; Sadykov, V.A.; Potapova, Y.V.; Salanov, A.N. Porous Al<sub>2</sub>O<sub>3</sub>/Al Metal Ceramics Prepared by the Oxidation of Aluminum Powder under Hydrothermal Conditions Followed by Thermal Dehydration: I. Composition and Macrocharacteristics of Composites. *Kinet. Catal.* **2000**, *41*, 826–834. [[CrossRef](#)]
23. Rai, A.; Park, K.; Zhou, L.; Zachariah, M.R. Understanding the mechanism of aluminum nanoparticle oxidation. *Combust. Theory Modell.* **2006**, *10*, 843–859. [[CrossRef](#)]
24. Vorozhtsov, A.B.; Lerner, M.; Rodkevich, N.; Nie, H.; Abraham, A.; Schoenitz, M.; Dreizin, E.L. Oxidation of nano-sized aluminum powders. *Thermochimica Acta* **2016**, *636*, 48–56. [[CrossRef](#)]
25. Antipina, S.A.; Zmanovskii, S.V.; Gromov, A.A.; Teipel, U. Air and water oxidation of aluminum flake particles. *Powder Technol.* **2017**, *307*, 184–189. [[CrossRef](#)]
26. Streletskii, A.N.; Kolbanov, I.V.; Borunova, A.B.; Butyagin, P.Y. Mechanochemical Activation of Aluminum: 3. Kinetics of Interaction between Aluminum and Water. *Colloid J.* **2005**, *67*, 631–637. [[CrossRef](#)]
27. Vlaskin, M.S.; Shkolnikov, E.I.; Lisicyn, A.V.; Bersh, A.V.; Zhuk, A.Z. Computational and experimental investigation on thermodynamics of the reactor of aluminum oxidation in saturated wet steam. *Int. J. Hydrog. Energy* **2010**, *35*, 1888–1894. [[CrossRef](#)]
28. Wang, H.Z.; Leung, D.Y.C.; Leung, M.K.H.; Ni, M. A review on hydrogen production using aluminum and aluminum alloys. *Renew. Sustain. Energy Rev.* **2009**, *13*, 845–853. [[CrossRef](#)]
29. Kravchenko, O.V.; Semenenko, K.N.; Bulychev, B.M.; Kalmykov, K.B. Activation of aluminum metal and its reaction with water. *J. Alloy. Compd.* **2005**, *397*, 58–62. [[CrossRef](#)]
30. Shmelev, V.; Nikolaev, V.; Lee, J.H.; Yim, C. Hydrogen production by reaction of aluminum with water. *Int. J. Hydrog. Energy* **2016**, *41*, 16664–16673. [[CrossRef](#)]
31. Shkolnikov, E.I.; Shaitura, N.S.; Vlaskin, M.S. Structural properties of boehmite produced by hydrothermal oxidation of aluminum. *J. Supercrit. Fluids* **2013**, *73*, 10–17. [[CrossRef](#)]
32. Lysenko, A.P.; Nalivayko, A.Y. Optimization of electrolysis during the high-pure aluminium oxide obtaining, using electrochemical method of aluminium oxidation. *Tsvetnye Met.* **2017**, *1*, 28–32. [[CrossRef](#)]
33. Nalivaiko, A.Y.; Lysenko, A.P.; Pak, V.I.; Ivanov, M.A. Feasibility Assessment for Leucosapphire Production from Aluminum Oxide Prepared Electrochemically. *Refract. Ind. Ceram.* **2018**, *55*, 80–84. [[CrossRef](#)]
34. Ilyukhina, A.V.; Kravchenko, O.V.; Bulychev, B.M. Studies on microstructure of activated aluminum and its hydrogen generation properties in aluminum/water reaction. *J. Alloy. Compd.* **2017**, *690*, 321–329. [[CrossRef](#)]
35. Ambaryan, G.; Valyano, G.; Zhuk, A.; Shkolnikov, E.; Gromov, A.; Zmanovsky, S.; Vlaskin, M. Partial oxidation of aluminum powder for obtaining a controlled amount of aluminum oxide on the surface of aluminum. *IOP Conf. Ser. Earth Env. Sci.* **2018**, *168*, 012021. [[CrossRef](#)]

36. Lisitsyn, A.V.; Dombrovsky, L.A.; Mendeleyev, V.Y.; Grigorenko, A.V.; Vlaskin, M.S.; Zhuk, A.Z. Near-infrared optical properties of a porous alumina ceramics produced by hydrothermal oxidation of aluminum. *Infrared Phys. Technol.* **2016**, *77*, 162–170. [[CrossRef](#)]
37. Grigorenko, A.V.; Ambaryan, G.N.; Valyano, G.E.; Vlaskin, M.S.; Gromov, A.A.; Zmanovsky, S.V. Kinetics of Aluminum Micron Powder Oxidation in Hot Distilled Water and Product Microstructure Investigation. *IOP Conf. Ser. Mater. Sci. Eng.* **2018**, *381*, 012028. [[CrossRef](#)]
38. Nie, H.; Schoenitz, M.; Dreizin, E.L. Oxidation of differently prepared Al-Mg alloy powders in oxygen. *J. Alloy. Compd.* **2016**, *685*, 402–410. [[CrossRef](#)]



© 2019 by the authors. Licensee MDPI, Basel, Switzerland. This article is an open access article distributed under the terms and conditions of the Creative Commons Attribution (CC BY) license (<http://creativecommons.org/licenses/by/4.0/>).